EURASIP Journal on Advances in Signal Processing

RESEARCH Open Access

Multiple fluctuating targets track-before-detect using multi-Bernoulli filter in radar sensor

Dongsheng Li[1], Sunyong Wu[1,2*], Honggao Deng[3], Xiyan Sun[2] and Ruhua Cai[1]

*Correspondence: wusunyong121991@163.com

[1] School of Mathematics and Computing Science, Guilin University of Electronic Technology, Guilin, China
[2] Guangxi Key Laboratory of Precision Navigation Technology and Application, Guilin, China
[3] Guangxi Key Laboratory of Wireless Wideband Communication and Signal Processing, Guilin, China

Abstract

This paper addresses the detection and tracking of multiple fluctuating targets for a track-before-detect algorithm based on the Multi-Bernoulli (MB-TBD) filter in surveillance radar systems. MB-TBD usually considers target amplitude information and ignores the fact that radar measurements are complex-valued. In this paper, we first propose to utilize phase information to improve the discrimination of targets from noise. More precisely, complex likelihood ratios are used instead of squared modulus measurements likelihood ratios for fluctuations of types Swerling 0, 1, 3. Secondly, the traditional MB-TBD filter cannot solve the problem of coexistence between targets with stronger amplitude and weaker amplitude when multiple fluctuating targets are moving. To address this limitation, an adaptive birth distribution based on joint successive target cancellation and measurement likelihood ratio driven is proposed. Moreover, in order to reduce computational complexity, the Bernoulli components of the same targets are merged after the MB-TBD updating. Finally, the proposed algorithm is implemented using Sequential Monte Carlo technology. The simulation results show that in challenging scenarios, the performance of the improved algorithm is better than the traditional algorithm, and it has a good application prospect.

Keywords: Track-before-detect, Weak targets, Amplitude fluctuation, Adaptive birth distribution, Multi-Bernoulli filter

1 Introduction

Traditional radar multi-target tracking (MTT) algorithms usually process the pre-processed data by compressing the single-frame data image into a finite set of points [1–3]. However, since the radar cross section (RCS) of the target fluctuates with the change of the viewing angle, the target's echo amplitude does not exceed the pre-processing threshold at certain moments which results in the loss of the potential target information. For weak targets, such as stealth aircraft, the problem is more serious. Unlike the traditional tracking algorithms, the track-before-detect (TBD) algorithm does not need to set a threshold, it is an effective method for weak target tracking. Most of the TBD implementation techniques are based on batch implementations, such as dynamic programming (DP) [4–7]; however, they are not suitable for real-time operations due to the

high computational complexity. A well-established real-time TBD approach is based on recursive implementations [8–10] of particle filtering (PF) algorithm. Nonetheless, the PF algorithm cannot solve the problem well that the number of targets in MTT is unknown and time-varying.

Another class of real-time TBD tracking is one of the methods that use random finite set (RFS). The MTT algorithm based on RFS theory solves the problems of the time-varying number of targets, data associations uncertainty, and detection uncertainty. The multi-Bernoulli (MB) filter [11–13] was another RFS-based MTT method proposed after the probability hypothesis density (PHD) filter [14–18] and the cardinalized PHD (CPHD) [19–21] filter. Compared to the two algorithms mentioned above, the MB filter has an advantage in terms of accuracy and computational complexity. It is worth noting that the above filters cannot provide identity information for multi-object estimation, and the existence of this problem drives the development of label RFS [22–24].

The key to the realization of MB-TBD is the calculation of the measurement likelihood ratio function (MLRF) based on the hidden state condition. It is worth noting that most MB-TBD algorithms in radar system choose the MLRF that only considers the amplitude information, i.e., square modulus measurement likelihood ratio (SLR) [25, 26]. For SLR that discard phase information, there are two ways to deal with the amplitude fluctuations. The first one is the overall likelihood ratio of the marginalized amplitude fluctuation density [27]. However, in practice this treatment is difficult to obtain an exact solution and can only be achieved using numerical approximation. The second way consists in marginalizing the likelihood in each cell independently [28]. The advantage of this heuristic second solution is that a closed form can be obtained. Unlike infrared and optical sensors, which receive real-valued measurements that contain only amplitude information, radar measurements are complex-valued, i.e., phase information in addition to amplitude information. The literature [29] shown that the phase loss leads to a filter sensitivity decrease.

In order to improve the recognition of targets from noise, Davey et al. [29] proposed a MLRF method containing phase information, called complex likelihood ratio (CLR). In addition, due to the change of target relative radar view and the influence of other unknown factors causing the target RCS to change, making the target amplitude information is fluctuating. Typical radar fluctuating targets include Swerling 0, 1, 3 [30]. The literatures [30, 31] introduce CLR into PF-TBD and DP-TBD, respectively, and consider a single target with fluctuation types of Swerling 0, 1 and 3. Single-target tracking of Swerling 0, 1, 3 target types in the Rayleigh sea clutter model was realized by the use of finite difference with continuous-discrete filtering in [32]. It is worth noting that the measurements used in [25] are square measurements.

In the detection and tracking of fluctuating targets, the existing research mainly introduces CLR into the filter to solve the problem of the single fluctuating target. Less research has been done for multiple fluctuating targets with unknown and time-varying target numbers. The problem of the co-existence of stronger and weaker amplitude targets can occur during multiple fluctuating targets movements. The traditional MB-TBD filter ignores targets with weak amplitudes, which leads to errors in the estimation of the target number. What is more serious is that the birth prior information of the target of traditional MB-TBD is known, which is inconsistent with most practical situations.

Although there are some measurement-based adaptive birth algorithms, such as the literature [25, 33] and so on. However, during the fluctuation process of the target amplitude, the amplitude information may be completely obscured in the noise for several consecutive frames. The maximum echo information received by the receiver may not be the surveillance target. When the fluctuating target reappears, the traditional MB-TBD filter will fail because the target prior information is unknown at this time.

To address the above issues, this paper extends the radar CLR method to MB-TBD, and embeds the assumption that target amplitude fluctuation follows the Swerling 0, 1, 3 model. Swerling statistical models belong to the RCS fluctuation statistical models, which are universal and include more radar target types. For example, Swerling 1 typical target such as small jet and Swerling 3 typical target such as helicopter. Specific contributions of this paper are given as follows.

Firstly, the expression of SLR with amplitude fluctuations of type Swerling 0, 1, 3 is modified, the expression of CLR considering phase information is given, and CLR is used as the likelihood ratio function of MB-TBD instead of SLR. The simulation results show that the MB-TBD algorithm-based CLR under amplitude fluctuation has better detection tracking performance than SLR, and it can reduce the complexity of the algorithm and run faster.

Secondly, in order to solve the problem that prior knowledge for target births is unknown, joint measurement likelihood ratio driven and successive-target-cancellation (STC)-based adaptive birth distribution for MB-TBD are proposed (LABer-STC-TBD), which is able to pick out the measurements that are likely to arise from real targets, so that the filter iteration can be maintained even when the target echo strength is covered below the noise.

Finally, after the update process, to account for the non-overlapping assumption, the overlapping estimates are merged. The Bernoulli components of the same target are merged at the end of the MB-TBD update, i.e., the trajectories are managed to estimate the correct number of targets after the MB-TBD filter is updated. The proposed trajectory management algorithm is more accurate and has lesser target estimation error.

The rest of the paper is organized as follows. Section 2 presents the multi-target state model under RFS, TBD measurement model, and the multi-target tracking problem under RFS. Section 3 gives the formulas for the CLR and the SLR under the amplitude fluctuation type Swerling 0, 1, 3. Section 4 presents the MB-TBD filter, the adaptive birth distribution and the trajectory merging model under the amplitude fluctuation type, and gives the SMC implementation. The experimental results are followed in Sect. 5. Results and discussion are given in Sect. 6. Finally, we conclude in Sect. 7.

2 Models and background

2.1 Multi-targets dynamic model

At time k, the kinematic state of the i-th individual target is represented by $\boldsymbol{x}_{k,i} = [x_{k,i}, \dot{x}_{k,i}, y_{k,i}, \dot{y}_{k,i}]^{\mathrm{T}}$, where $(x_{k,i}, y_{k,i})$ and $(\dot{x}_{k,i}, \dot{y}_{k,i})$, respectively, denote the ith target position and velocity, T denotes the matrix transpose. For the multi-target tracking problem, since the number of targets is an unknown and random variable, the ranking of target states has no physical significance, so the state of the multi-target X_k can be expressed as a random finite set (RFS) [11], which is defined as follows

$$X_k = \{\boldsymbol{x}_{k,1}, \boldsymbol{x}_{k,2}, \ldots, \boldsymbol{x}_{k,N_k}\} \in F(\mathcal{X}). \tag{1}$$

where $\mathcal{F}(\mathcal{X})$ denote the collection of all subsets of state space $\mathcal{X}$, and N_k denote the number of targets at time k.

The dynamics model of multi-target state can be expressed as:

$$X_k = \left[\bigcup_{\boldsymbol{\zeta}\in X_{k-1}} S_{k|k-1}(\boldsymbol{\zeta})\right] \cup \left[\bigcup_{\boldsymbol{\zeta}\in X_{k-1}} B_{k|k-1}(\boldsymbol{\zeta})\right] \cup \Gamma_k. \tag{2}$$

where X_k is the multi-target state set at time k, $S_{k|k-1}(\boldsymbol{\zeta})$ is surviving RFS of target at time k that evolves from a target with previous state $\boldsymbol{\zeta}$, $B_{k|k-1}(\boldsymbol{\zeta})$ is the spawning RFS of target at time k, Γ_k is the RFS of spontaneous births at time k. In addition, it is assumed that each RFS in (2) is independent of each other.

2.2 Measurement model

In this paper we considered radar sensor is an active monopulse radar, with a linear phased array antenna. In the TBD algorithm, the sensor provides a two-dimensional image of the surveillance area at intervals T, the surveillance region scenario considered in this paper is shown in Fig. 1. As shown in Fig. 1, every image consists of $N_c = N_r \times N_\theta$ resolution cells [30]. The measurement matrix can also be denote as a vector form $\boldsymbol{Z_k} = [z_k^{(1)}, z_k^{(2)}, \ldots, z_k^{(N_c)}]$. The measurement $z_k^{(j)}$ can be denoted as [30],

$$z_k^{(j)} = \begin{cases} \sum_{i=1}^{N_k} \rho_{k,i} e^{j\varphi_{k,i}} h_k{}^{(j)}(\boldsymbol{x}_{k.i}) + \omega_k^{(j)} & H_1 \\ \omega_k^{(j)} & H_0 \end{cases} \tag{3}$$

where $\omega_k^{(j)}$is the complex Gaussian noise with covariance Γ. $\varphi_{k,i}$ is the unknown phase assumed to be uniformly distributed over the interval $[0, 2\pi)$ at time k. $h_k{}^{(j)}(\boldsymbol{x}_{k.i})$ denotes the contribution intensity from the target cell j. H_1 denote the assumption that there are N_k targets, and H_0 denote that there is no target. $\rho_{k,i}$ is the amplitude of the target, in

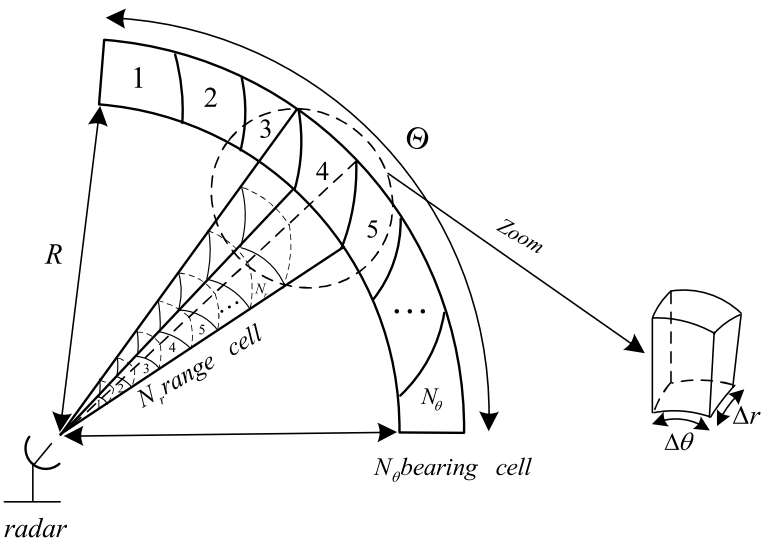

Fig. 1 Radar surveillance region illustration

this paper, which is modeled using the Swerling family of target amplitude fluctuation models, i.e.,

1 Under the Swerling 0 model, the amplitude $\rho_{k,i}$ of each target is equal to the parameter ρ_i.
2 For the Swerling 1 model, the amplitude $\rho_{k,i}$ of the target is assumed to submit to a Rayleigh distribution, $\mathrm{E}[\rho_{k,i}^2] = 2\sigma_{\rho_i}^2$, the PDF of $\rho_{k,i}$ is as follows

$$p_{Sw1}(\rho_{k,i}) = \frac{\rho_{k,i}}{\sigma_{\rho_i}^2} \exp\left(-\frac{\rho_{k,i}^2}{2\sigma_{\rho_i}^2}\right) \tag{4}$$

.

3 When the amplitude fluctuation type is Swerling 3 and $\rho_{k,i}$ follows a chi-square distribution with four degrees of freedom, $\mathrm{E}\left(\rho_{k,i}^2\right) = \nu_{\rho_i}$, the PDF of $\rho_{k,i}$ is as follows

$$p_{Sw3}\left(\rho_{k,i}\right) = \frac{8\rho_{k,i}^3}{\nu_{\rho_i}^2} \exp\left(-\frac{2\rho_{k,i}^2}{\nu_{\rho_i}}\right) \tag{5}$$

For equation 3, range and bearing radar covering the surveillance area in polar coordinates are considered. For the range, it is assumed that the transmitted pulse is a linear frequency modulated signal with bandwidth B and duration T_e, and the range ambiguity function is given by the [34]

$$h_r^l(\boldsymbol{x}_{k,i}) = \frac{\sin\left(\pi B\tau^l\left(1 - \frac{\left|\tau^l\right|}{T_e}\right)\right)}{\pi B\tau^l}, \left|\tau^l\right| \le T_e \tag{6}$$

where $\left|\tau^l\right| = 2(r_k - r_l)/c$, c is the speed of electromagnetic waves; $r_k = \sqrt{x_{k,i}^2 + y_{k,i}^2}$, $r_l = r_{\min} + \left(l + \frac{1}{2}\right)\Delta_r, l \in [0, N_r - 1], \Delta_r = \frac{c}{2B}$ is range resolution.

At the receiver side, the radar consists of a linear phased array, where the spacing of the N_a antenna is $\frac{\lambda}{2}$ and λ is the wavelength of the carrier frequency. Then the bearing ambiguity function is given by the [31] as

$$h_\theta^m(\boldsymbol{x}_{k,i}) = \frac{\sin\left(\frac{N_a\Phi^m}{2}\right)}{N_a \sin\left(\frac{\Phi^m}{2}\right)} \tag{7}$$

where $\Phi^m = \pi[\sin(\theta_k) - \sin(\theta_m)]$, $\theta_k = \arctan\left(\frac{y_k}{x_k}\right)$, $\theta_m = \theta_{\min} + \left(m + \frac{1}{2}\right)\Delta_\theta$, $m \in [0, N_\theta - 1], \Delta_\theta = 1.722\frac{\lambda}{N_a}$ represents the half-power beamwidth.

The ambiguity function in the range-bearing cell (l, m) is

$$h^{(j)}(\boldsymbol{x}_k) = h_r^l(\boldsymbol{x}_k) \times h_\theta^m(\boldsymbol{x}_k) \tag{8}$$

The set of complete measurements collected up to time is given by

$$Z_{1:k} = \{Z_i, i = 1, 2 \ldots k\} \tag{9}$$

2.3 The optimal Bayesian filter

The finite sets statistics (FISST) proposed by Mahler provides a mathematical framework for the problem of detection, tracking and classification of multi-target under unified Bayesian paradigm [11]. In FISST framework, given the measurements Z_k at time k and the history of measurements $Z_{1:k-1}$, then the optimal multi-target Bayesian filter propagates RFS based on the posterior probability density $p_{k|k}(X_k|Z_{1:k})$, its prediction and updating steps are as follows

$$p_{k|k-1}(X_k|Z_{1:k-1}) = \int p_{k|k-1}(X_k|X_{k-1})p_{k-1}(X_{k-1}|Z_{1:k-1})\delta X_{k-1} \tag{10}$$

$$p_{k|k}(X_k|Z_{1:k}) = \frac{p_k(Z_k|X_k)p_{k|k-1}(X_k|Z_{1:k-1})}{\int p_k(Z_k|X_k)p_{k|k-1}(X_k|Z_{1:k-1})\delta X_k} \tag{11}$$

where considering the function f: $\mathcal{F}(\mathcal{X}) \to \mathbb{R}$, $\mathcal{F}(\mathcal{X})$ denotes the set containing all subsets of $\mathcal{X}$, the integral of the function f over a closed subset S of $\mathcal{X}$ is given by

$$\int_S f(X)\delta X = \sum_{n=0}^{\infty} \frac{1}{n!} \int_{\underbrace{S \times \cdots \times S}_{ntimes}} f(\{x_1, \ldots, x_n\}) \mathrm{d}x_1 \cdots \mathrm{d}x_n \tag{12}$$

TBD uses the raw measurements generated by sensor. The measurement is an image composed of thousands or even millions of pixels, however the target does not affect all the pixels, but only occupies a small area of the image, which leads to an estimation of inefficient if we use $p(\boldsymbol{Z_k}|X_k)$ directly. Define the proportion of the likelihood $p(\boldsymbol{Z_k}|X_k)$ of the existing target to the likelihood $p_0(\boldsymbol{Z_k})$ of no target [29].

$$L_z(\boldsymbol{Z_k}|X_k) = \frac{p(\boldsymbol{Z_k}|X_k)}{p_0(\boldsymbol{Z_k})} \tag{13}$$

It can be seen from the (13) that the calculation of the likelihood ratio is limited to the area around the target, which improves the efficiency of the calculation.

2.4 Basic MB-TBD filter

A MB RFS X is a union of M independent Bernoulli RFS X that represents a fixed number M of targets. Therefore, the set $\left\{r^{(i)}, p^{(i)}\right\}_{i=1}^{M}$ denotes the MB RFS, where $r^{(i)}$ is existence probability and $p^{(i)}$ is the spatial distribution of the i-th Bernoulli distribution. The probability density $\pi(X)$ of a MB RFS is given by [11]

$$\pi(\{x_1, \ldots x_n\}) = \prod_{j=1}^{M}(1 - r^j) \times \sum_{1 \le i_1 \ne \cdots \ne i_n \le M} \prod_{j=1}^{n} \frac{r^{(i_j)} p^{(i_j)}(x_j)}{1 - r^{(i_j)}} \tag{14}$$

In [20], it is shown that the MB filtering method under RFS provides an accessible solution to the multi-target estimation problem for image measurements. If the posterior probability density π_{k-1} is in the form of MB, then the prediction $\pi_{k|k-1}$ and the update $\pi_{k|k}$ in the case of non-overlapping targets will also to be in the form of MB. Hence, the prediction (10) and the update (11) can be approximated in the following way.

MB-TBD prediction: Given the posterior MB -TBD parameters $\pi_{k-1} = \left\{\left(r_{k-1}^{(i)}, p_{k-1}^{(i)}\right)\right\}_{i=1}^{M_{k-1}}$ at time $k-1$, the predict MB-TBD parameters are

$$\pi_{k|k-1} = \left\{\left(r_{P,k|k-1}^{(i)}, p_{P,k|k-1}^{(i)}\right)\right\}_{i=1}^{M_{k-1}} \cup \left\{\left(r_{\Gamma,k}^{(i)}, p_{\Gamma,k}^{(i)}\right)\right\}_{i=1}^{M_{\Gamma,k}} \tag{15}$$

where

$$r_{P,k|k-1}^{(i)} = r_{k-1}^{(i)} \left\langle p_{k-1}^{(i)}, p_{S,k} \right\rangle \tag{16}$$

$$p_{P,k|k-1}^{(i)}(\boldsymbol{x}) = \frac{\left\langle f_{k|k-1}(\boldsymbol{x} \mid \cdot), p_{k-1}^{(i)} p_{S,k} \right\rangle}{\left\langle p_{k-1}^{(i)}, p_{S,k} \right\rangle} \tag{17}$$

where given previous state $\boldsymbol{\zeta}$, $f_{k|k-1}(\cdot \mid \boldsymbol{\zeta})$ and $p_{S,k}(\boldsymbol{\zeta})$ denote the single target transition density and probability of target existence at time k, respectively. $\left\{\left(r_{\Gamma,k}^{(i)}, p_{\Gamma,k}^{(i)}\right)\right\}_{i=1}^{M_{\Gamma,k}}$ is parameters of the MB RFS of births at time k.

MB-TBD update: Given the predict MB-TBD parameters $\pi_{k|k-1} = \left\{\left(r_{k-1}^{(i)}, p_{k-1}^{(i)}\right)\right\}_{i=1}^{M_{k|k-1}}$, the update MB-TBD parameters are

$$\pi_k = \left\{\left(r_k^{(i)}, p_k^{(i)}\right)\right\}_{i=1}^{M_{k|k-1}} \tag{18}$$

where

$$r_k^{(i)} = \frac{r_{k|k-1}^{(i)} \left\langle p_{k|k-1}^{(i)}, L_z \right\rangle}{1 - r_{k|k-1}^{(i)} + r_{k|k-1}^{(i)} \left\langle p_{k|k-1}^{(i)}, L_z \right\rangle} \tag{19}$$

$$p_k^{(i)} = \frac{p_{k|k-1}^{(i)} L_z}{\left\langle p_{k|k-1}^{(i)}, L_z \right\rangle} \tag{20}$$

Each pixel cell received by the radar sensor is a complex random variable containing both amplitude and phase information. The existing MB-TBD algorithm is the problem of target tracking in the non-fluctuating target, where the implementation only considers the amplitude information and ignores the phase information. In this paper, we consider two implementations of MB-TBD in the case of target amplitude fluctuation, one is the SLR under the squared radar measurement, and the other is the CLR under the consideration of phase information.

3 Calculation of the SLR and CLR

The measurement (3) contains the unknown phase $\varphi_{k,i}$ and amplitude $\rho_{k,i}$ of the target. They are unknown, therefore, the likelihood $p(\boldsymbol{Z_k}|X_k)$ or $p\left(|\boldsymbol{Z}_k|^2 \middle| X_k\right)$ cannot be directly calculated, and the phase $\varphi_{k,i}$ and amplitude $\rho_{k,i}$ need to be marginalized.

3.1 Calculation of the SLR

Denote the squared modulus vector of the complex measure is $|\boldsymbol{Z}_k|^2 = \left[\left|z_k^{(1)}\right|^2, \left|z_k^{(2)}\right|^2, \ldots, \left|z_k^{(N_c)}\right|^2\right]$. Assuming that pixel values are distributed independently and that the target's influence area does not overlap, then,

$$p\left(|\boldsymbol{Z}_k|^2 \middle| x_k\right) = \prod_{j=1}^{N_c} p\left(\left|z_k^{(j)}\right|^2 \middle| \boldsymbol{x}_k\right) \tag{21}$$

When the target does not exist, the likelihood $p_0(\boldsymbol{Z}_k)$ is [29]

$$p_0\left(|\boldsymbol{Z}_k|^2\right) = \prod_{j=1}^{N_c} \frac{\left|z_k^{(j)}\right|}{\sigma_n^2} \cdot \exp\left(-\frac{\left|z_k^{(j)}\right|^2}{2\sigma_n^2}\right) \tag{22}$$

(1) For Swerling 0, the L_z can be written as [29]

$$L_z\left(|\boldsymbol{Z}_k|^2 \middle| \boldsymbol{x}_k\right) = \prod_{j=1}^{N_c} \exp\left(-\frac{\rho_i^2\left|h_k^{(j)}\right|^2}{2\sigma_n^2}\right) \times I_0\left(\frac{\rho_i\left|h_k^{(j)} z_k^{(j)}\right|}{\sigma_n^2}\right) \tag{23}$$

where $\mathrm{I}_0(\cdot)$ is the modified Bessel function of the first kind.

(2) Modify the L_z of the Swerling 1 model in the literature [30], then,

$$\begin{aligned} L_z\left(|Z_k|^2 \middle| x_k\right) &= \prod_{j=1}^{N_c} \int_0^{+\infty} \frac{p\left(\left|z_k^{(j)}\right|^2 \middle| x_k, \rho\right)}{p_0\left(\left|z_k^{(j)}\right|^2\right)} p(\rho)\mathrm{d}\rho \\ &= \prod_{j=1}^{N_c} \int_0^{+\infty} \exp\left(-\frac{\rho_i^2\left|h_k^{(j)}\right|^2}{2\sigma_n^2}\right) \times I_0\left(\frac{\rho_i\left|h_k^{(j)} z_k^{(j)}\right|}{\sigma_n^2}\right) p_{Sw1}\mathrm{d}\rho \end{aligned} \tag{24}$$

then,

$$L_z\left(|\boldsymbol{Z}_k|^2 \middle| \boldsymbol{x}_k\right) = \prod_{j=1}^{N_c} \frac{\sigma_n^2}{\lambda_k^{(j)}} \exp\left(\frac{\sigma_{\rho_i}^2\left|z_k^{(j)}\right|^2\left|h_k^{(j)}\right|^2}{2\sigma_n^2\lambda_k^{(j)}}\right) \tag{25}$$

where $\lambda_k^{(j)} = \sigma_n^2 + \sigma_{\rho_i}^2\left|h_k^{(j)}\right|^2$.

(3) Different from the expression of L_z by Swerling 3 in [30], this paper re-derives Swerling 3,

$$L_z\left(|\boldsymbol{Z}_k|^2 \middle| \boldsymbol{x}_k\right) = \prod_{j=1}^{N_c} \frac{2\sigma_n^2}{1 + \frac{v_{\rho_i}\left|h_k^{(j)}\right|^2}{(4\sigma_n^2)^2}} \left(1 + \frac{\frac{\left|z_k^{(j)}\right|^2}{2\sigma_n^2}}{1 + \frac{4\sigma_n^2}{v_{\rho_i}\left|h_k^{(j)}\right|^2}}\right) \times \exp\left(\frac{1}{1 + \frac{v_{\rho_i}\left|h_k^{(j)}\right|^2}{4\sigma_n^2}}\right) \tag{26}$$

where the derivation of Eq. (25) is analogous to Eq. (23).

3.2 Calculation of the CLR

The SLR of the square measurement does not consider the spatial coherence of the complex measurement, and for the case of amplitude with no fluctuation, the SLR also needs to calculate a Bessel function with a significant point spread function contribution for each pixel. Experience shows that the calculation of the Bessel function is the most computationally expensive part of the TBD algorithm. In summary, SLR using squared measures is not optimal, in order to avoid these drawbacks, in [29–32], the joint likelihood of the entire sensor image is given, taking into account the spatial coherence of the phase and spatially correlated noise. The calculation of CLR not only improves the performance of target detection and tracking, but also effectively reduces the computational complexity.

The likelihood $p_0(\boldsymbol{Z}_k)$ of no target is [29]

$$p_0(\boldsymbol{Z}_k) = \frac{1}{\sqrt{2\pi \det(\Gamma)}} \exp\left\{-\frac{1}{2}\boldsymbol{Z}_k^{\mathrm{H}}\Gamma^{-1}\boldsymbol{Z}_k\right\} \tag{27}$$

This subsection gives the expression for the CLR for the three Swerling types [30].

(1) Swerling 0,

$$L_z(\boldsymbol{Z}_k|\boldsymbol{x}_k) = \exp\left(-\rho_i^2 h_k^{\mathrm{H}}\Gamma^{-1}h_k\right) I_0\left(2\rho_i\left|h_k^{\mathrm{H}}\Gamma^{-1}\boldsymbol{Z}_k\right|\right) \tag{28}$$

(2) Swerling 1,

$$L_z(\boldsymbol{Z}_k|\boldsymbol{x}_k) = \frac{1}{1+2\sigma_{\rho_i}^2 h_k^{\mathrm{H}}\Gamma^{-1}h_k} \exp\left(\frac{2\sigma_{\rho_i}^2\left|h_k^{\mathrm{H}}\Gamma^{-1}\boldsymbol{Z}_k\right|^2}{1+2\sigma_{\rho_i}^2 h_k^{\mathrm{H}}\Gamma^{-1}h_k}\right) \tag{29}$$

(3) Swerling 3,

$$L_z(\boldsymbol{Z}_k|\boldsymbol{x}_k) = \frac{4}{\left(2+\nu_{\rho_i} h_k^{\mathrm{H}}\Gamma^{-1}h_k\right)^2} \times \left(1+\frac{\nu_{\rho_i}\left|h_k^{\mathrm{H}}\Gamma^{-1}\boldsymbol{Z}_k\right|}{2+\nu_{\rho_i} h_k^{\mathrm{H}}\Gamma^{-1}h_k}\right) \times \exp\left(\frac{\nu_{\rho_i}\left|h_k^{\mathrm{H}}\Gamma^{-1}\boldsymbol{Z}_k\right|^2}{2+\nu_{\rho_i} h_k^{\mathrm{H}}\Gamma^{-1}h_k}\right) \tag{30}$$

4 Implementation issues

4.1 Adaptive birth distribution of MB-TBD filter with amplitude fluctuating targets

The traditional MB-TBD assumes that the birth RFS is known as a priori and initializes the multi-Bernoulli filter with a priori knowledge (KpMB-TBD). However, when the prior knowledge is completely unknown and the SNR is low, the continuous miss-detection of MB components, may lead to the ineffective of KpMB-TBD. For the environments of low SNR, missed detection is a common phenomenon. If the birth target appears in a state area that is not covered by the true target birth intensity, it is difficult for KpMB-TBD to find the targets, even if a large number of birth targets cover the whole space. The general strategy is to let the birth distribution cover the total scenario. However, this requires a large number of particles to represent the birth model, this method is very inefficient although it is feasible.

In [25, 32], it is shown that for the MB filter, the adaptive birth distribution must follow the MB distribution, and the MB birth distribution $\pi_{\Gamma,k}$ at time $k+1$ depends on the measurement $\boldsymbol{Z}_k$ at the previous moment, i.e.,

$$\pi_{\Gamma,k+1} = \left\{ r_{\Gamma,k}^{(i)}(z), p_{\Gamma,k}^{(i)}(x|z) \right\}_{i=1}^{|\boldsymbol{Z}_k|} \tag{31}$$

Then the existence probability of each Bernoulli component is

$$r_{\Gamma,k}(z) = \min\left(r_{\Gamma,\max}, \frac{1 - r_{U,k}(z)}{\sum_{\xi \in Z_k} 1 - r_{U,k}(\xi)} \cdot \lambda_{\Gamma,k+1|k} \right) \tag{32}$$

$$r_{U,k}(x) = \sum_{\ell=1}^{M_{k|k-1}} \frac{r_{k|k-1}^{(\ell)} \left\langle p_{k|k-1}^{(\ell)}, L_z \right\rangle}{1 - r_{k|k-1}^{(\ell)} + r_{k|k-1}^{(\ell)} \left\langle p_{k|k-1}^{(\ell)}, L_z \right\rangle}$$

where $\lambda_{\Gamma,k+1|k}$ is the expected number of targets for newborn at time $k+1$ and $r_{\Gamma,\max} \in [0,1]$. Since the mean cardinality of MB RFS is given by the sum of the existence probabilities, the mean cardinality of the new birth targets is

$$\sum_{\xi \in Z_k} r_{\Gamma,k}(\xi) \leq \lambda_{\Gamma,k+1|k} \tag{33}$$

For target kinematics of amplitude fluctuation, the target intensity will change at any time. In the target tracking process, the weaker target is often ignored, which leads to an error in the estimation of the number of targets. Figures 2 and 3 show that in the case of SNR=8dB, considering the influence of noise on the target amplitude fluctuation type Swerling 3.

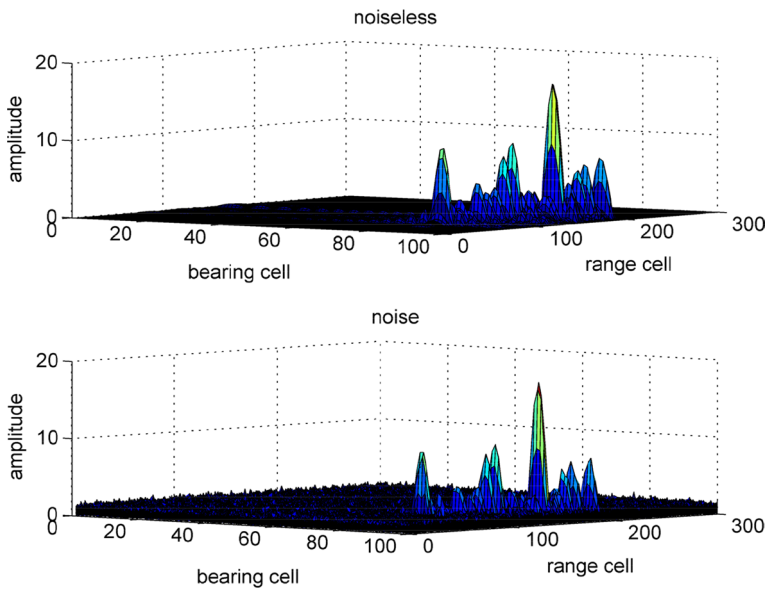

Fig. 2 The target amplitude fluctuation schematic. Top: Noiseless. Bottom: SNR=8dB

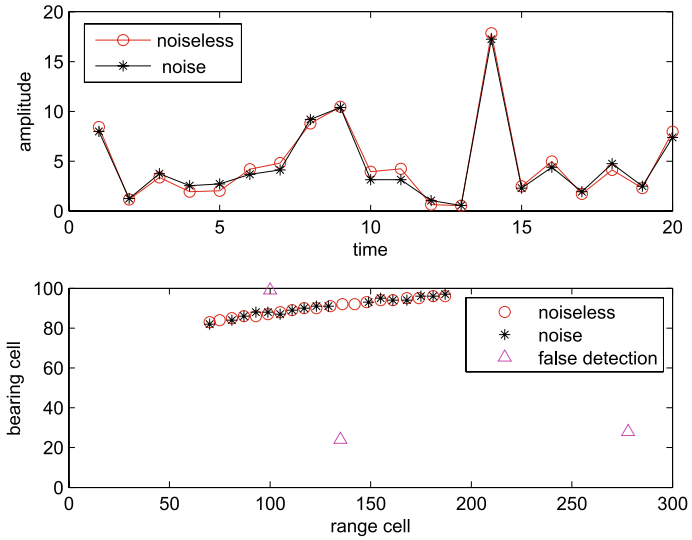

Fig. 3 The schematic diagram of the target amplitude. Top: Target amplitude fluctuation. Bottom: The highest echo intensity position

Figure 2 shows the type of target amplitude fluctuations Swerling 3 under noiseless and SNR=8dB. The truth target amplitude with time is indicated in Fig. 3 top, and Fig. 3 bottom shows the strongest echo position in both backgrounds. Figures 2 and 3 intuitively reflects that for Swerling 3 type, the target echo is completely swamped by noise at part of the time, which may lead to the ineffective of filter when the a priori information is known. Also, for fluctuating targets, the maximum echo information detected by the receiver in a low SNR environment may be non-surveillance targets, which will affect the judgment of the filter. While for Swerling 0 type with no fluctuation of the target, the real target echo amplitude is stable. The above only draws the fluctuation of Swerling 3, for another fluctuation of Swerling 1, the target amplitude fluctuation range is still very wide. It is also important to pay attention to the fact that in amplitude fluctuation multi-target tracking, the amplitude among targets are different, and the target with stronger echoes will affect the target with weaker echoes, and the KpBer-TBD cannot solve the amplitude fluctuation problems of weak multi-target tracking.

In order to solve the above difficulties, this section draws on the idea of successive-target-cancellation (STC) in [35], by making a balance between low false alarm rate and high detection probability, and proposes a MB-TBD based on measurement likelihood adaptive birth distribution (LABer-STC-TBD).

To facilitate the following calculations, transform vector $\boldsymbol{Z}_k$ into matrix Z_k, i.e.,

$$Z_k = \begin{bmatrix} z_k^{(1,1)} & z_k^{(1,2)} & \cdots & z_k^{(1,N_\theta)} \\ z_k^{(2,1)} & z_k^{(2,2)} & \cdots & z_k^{(2,N_\theta)} \\ \vdots & \vdots & \ddots & \vdots \\ z_k^{(N_r,1)} & z_k^{(N_r,2)} & \cdots & z_k^{(N_r,N_\theta)} \end{bmatrix} \tag{34}$$

The idea of LABer-STC-TBD firstly select previous instants measurements to generate birth targets adaptively, and not all measurement information is used to drive the birth distribution, i.e.,

$$\tilde{Z}_k = \left\{ z_k^{(l,m)} \middle| \left| z_k^{(l,m)} \right|^2 > \gamma \right\} \tag{35}$$

The threshold γ can be calculated by giving the false alarm P_{fa} of the resolution cell, the threshold γ is used to avoid information redundancy and to discard measurements that may originate from noise or clutter. In this paper, a threshold γ more suitable for the case of target fluctuation is modified on the basis of the [36].

$$\gamma = -2\mathrm{E}[\rho_k^2] \log P_{\text{fa}} \tag{36}$$

Since each Bernoulli component represents a target, and this paper considers target detection and tracking in the case of non-overlapping targets, the measurements are divided after selection so that the particles in each cluster are generated from measurements around the target diffusion location, which not only avoids particle clutter in the components but also reduces the overlapping components as much as possible. The adaptive birth distribution can be expressed as

$$\pi_{\Gamma,k+1} = \left\{ r_{\Gamma,k}^{(i)}(\tilde{z}), p_{\Gamma,k}^{(i)}(x|\tilde{z}) \right\}_{i=1}^{\left|\tilde{Z}_k\right|} \tag{37}$$

$$r_{\Gamma,k}(\tilde{z}) = \min \left(r_{\Gamma,\max}, \frac{1 - r_{U,k}(\tilde{z})}{\sum_{\xi \in \tilde{Z}_k} 1 - r_{U,k}(\xi)} \cdot \lambda_{\Gamma,k+1|k} \right) \tag{38}$$

Using (37) to calculate the existence probability of each cluster, the Bernoulli components whose existence probability less than 0.5 are eliminated. The detected component is used to modify the existing measurement to eliminate the influence of the component on the detection of the remaining target. When the detected target acts on the resolution cell (l, m), the measurement of the resolution cell (l, m) after eliminating the effect of this target

$$\bar{z}_k^{(l,m)} = Z_k - z_k^{(l,m)} \tag{39}$$

At this point the sensor gets the repaired measurement set within the whole $N_r \times N_\theta$ scenario as

$$Z_k = \left[\bar{z}_k^{(l,m)} \right], \quad l = 1, 2, \ldots N_r, m = 1, 2, \ldots N_\theta \tag{40}$$

After returning to the above steps and increasing the false alarm rate until the presence probability of all Bernoulli components is below 0.5. It is important to note that (39) holds because (3) of the measurement equation is established and the assumption that the target contribution to the intensity is additive. A modification of (39) is needed for the measurements that are not additive models. Algorithm 1 gives the LABer-STC-TBD algorithm for adaptive birth multi-Bernoulli density $\left\{ \left(r_{\Gamma,k}^{(i)}, p_{\Gamma,k}^{(i)} \right) \right\}_{i=1}^{M_{\Gamma,k}}$.

Algorithm 1 LABer-STC-TBD pseudo code

1: **Input:** Measurement Z_k
2: **while** 1 **do**
3: Calculate the threshold γ using (36) and (37) to select the measurement.
4: Grouping pixel positions of the same target, and eliminating the set with one element in the group, i.e., the measurements after screening are $\hat{Z}$.

$$\hat{Z}=\left\{\left\{\left(l_1^j,m_1^j\right)\right\}_{j=1}^{N_1},\left\{\left(l_2^j,m_2^j\right)\right\}_{j=1}^{N_2},\ldots,\left\{\left(l_i^j,m_i^j\right)\right\}_{j=1}^{N_i},\ldots,\left\{\left(l_T^j,m_T^j\right)\right\}_{j=1}^{N_K}\right\},\left|\left\{\left(l_i^j,m_i^j\right)\right\}\right|>1$$

5: For each of the $\left\{\left(l_i^j,m_i^j\right)\right\}_{j=1}^{N_i}$, translate to the target position in the Cartesian coordinate system: $r_i^j=r_{\min}+\left(l_i^j+\frac{1}{2}\right)\Delta_r$, $\theta_i^j=\theta_{\min}+\left(m_i^j+\frac{1}{2}\right)\Delta_\theta$, $x_i^j=r_i^j\cos\theta_i^j, y_i^j=r_i^j\sin\theta_i^j$.
6: The target state is expressed as

$$ZZ\triangleq\left\{\left\{\left(x_1^j,y_1^j\right)\right\}_{j=1}^{N_1},\left\{\left(x_2^j,y_2^j\right)\right\}_{j=1}^{N_2},\ldots\left\{\left(x_T^j,y_T^j\right)\right\}_{j=1}^{N_K}\right\}$$

7: The i-th birth Bernoulli component of the particle is $x_{\Gamma,k}^i=\left[x_i^j,v_x,y_i^j,v_y\right]^T$, and its corresponding weight is $\tilde{w}_{\Gamma,k}^i=\frac{1}{N_{filter}}$, $r_{\Gamma,k}^{(i)}=r_{start}$.
8: Update the birth Bernoulli component using (19) and (20).
9: **if** $r_{\Gamma,k}^{(i)}<0.5$ **then**
10: Delete i-th birth Bernoulli component.
11: **else**
12: Using (38) to calculate the existence probability $r_{\Gamma,k+1}^{(i)}$, $\tilde{w}_{\Gamma,k+1}^i=\tilde{w}_{\Gamma,k}^i$.
13: **end if**
14: **if** $\mathrm{sum}(r_{\Gamma,k+1})==0$ **then**
15: break
16: **else**
17: $Z_k=Z_k-\hat{Z}$, $P_{fa}=P_{fa}+0.1$.
18: **end if**
19: **end while**
20: **Output:** $\left\{\left(r_{\Gamma,k+1}^{(i)},p_{\Gamma,k+1}^{(i)}\right)\right\}_{i=1}^{M_{\Gamma,k+1}}$

Note: In Step 4, each $\left\{\left(l_i^j,m_i^j\right)\right\}_{j=1}^{N_i}$ denotes the location of the target energy scattered to the surroundings, and the selected measurements are divided into N_K classes based on the distance, i.e., for any $A=\left\{\left(l_i^j,m_i^j\right)\right\}_{j=1}^{N_i}$, $B=\left\{\left(l_k^j,m_k^j\right)\right\}_{j=1}^{N_k}$, there are: $A,B\in\hat{Z}$, $A\cap B=\emptyset$, and for any element in A are in the circle whose radius is R (R is set by the target diffusion intensity) and the center is $\left(\frac{l_i^1+l_i^2+\ldots l_i^{N_i}}{N_i},\frac{m_i^1+m_i^2+\ldots m_i^{N_i}}{N_i}\right)$. The number of elements in $\hat{Z}$ with 1 is eliminated, i.e., the positions with no energy scattering are eliminated. Figure 4 reflects the point spreading of the target. Figure 4a indicates that the target energy spreads to the neighboring pixels around the target location with little spillover to more distant locations, and the white circle in the image is centered on the target location. Figure 4b indicates the measurement from the receiver with SNR = 10 dB.

As can be seen from Fig. 4, the real target affects the surrounding pixel locations, while the noise locations are disorderly, even if the SNR is so low that the target location intensity is treated as noise in the first cycle, there is a chance of detecting the real target after the repair of the measurement. In Step 5–6, the target distance and bearing are converted to

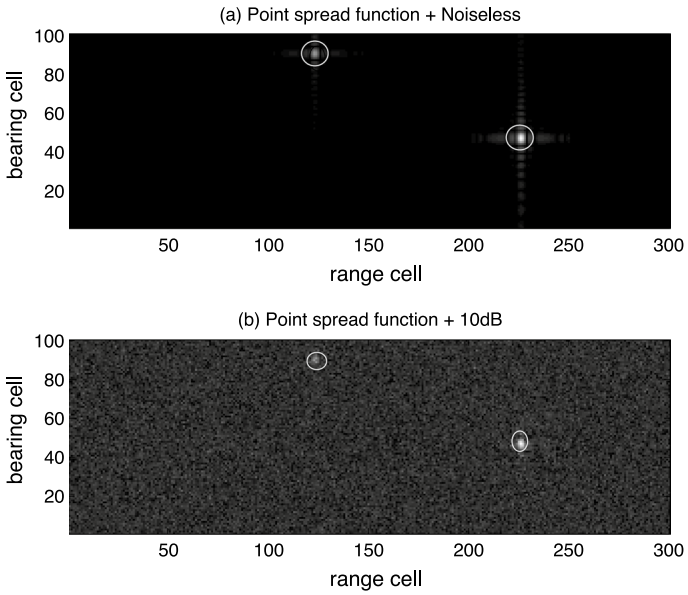

Fig. 4 Measurement diagram

positions in Cartesian coordinates, and the SMC implementation is considered to generate particles in the near of the real target. In Step 7, $r_{\Gamma,k}^{(i)} = r_{start}$ is to cope with the update in Step 8-13, not the existence probability of the birth component, which is calculated based on equation 37, and the birth particle in Step 7 is not in the position of selection measurement, but contains some disturbances, the reason is that the target will be affected by noise in the process of moving, which will add some disturbances to prevent the estimated target from leaving the real trajectory in the moving process. Remove the Bernoulli components with the existence probability lower than 0.5 in the Step 8–13 and Step 14–18, if it leads to the disappearance of all components, then the search is over, otherwise the target location information will be found and the surrounding pixels will be eliminated for the next iteration. It should be noted that in the first search process, if $N_i = 1, i = 1, 2 \ldots, N$, then it shows that there is no newborn target at this time, and the MB filter will continue to iterate to the next moment with surviving targets.

4.2 Track merging

After the update of traditional MB-TBD, the Bernoulli components whose existence probability lower than the threshold H_{merge} will be discarded, so as to reduce the increase of Bernoulli components. To solve the problem of linear growth of Bernoulli components after updating, an algorithm for trajectory merging based on distance and particle weights is proposed.

The Bernoulli component within the threshold represents the same target, then the MB components can be expressed as:

$$\left\{ \left\{ \left(r_k^{(i)}, p_k^{(i)} \right) \right\}_{i=1}^{M_1}, \left\{ \left(r_k^{(i)}, p_k^{(i)} \right) \right\}_{i=1}^{M_2} \cdots \left\{ \left(r_k^{(i)}, p_k^{(i)} \right) \right\}_{i=1}^{M_N} \right\} \tag{41}$$

where $M_1 + M_2 + \cdots M_N = M_{k|k}$, and $\left\{\left(r_k^{(i)}, p_k^{(i)}\right)\right\}_{i=1}^{M_j}, j = 1, 2, \ldots M_{k|k}$ denotes the Bernoulli components of the same target, the $M_{k|k}$ components are divided into a total of M_N classes, $1 \leq M_j \leq M_N$.

Subsequently, the components with the highest existence probability of the same target are reserved, then the Bernoulli components before selection are denoted as $\left\{\left(r_k^{(i)}, p_k^{(i)}\right)\right\}_{i=1}^{M_j}$, and there will be only one component of the same target after selection, i.e.,

$$\left\{\left(r_k^{(i_j)}, p_k^{(i_j)}\right)\right\}, r_k^{(i_j)} = \max(r_k^{(1)}, r_k^{(2)} \ldots, r_k^{(M_j)}) \tag{42}$$

where $\left|\left\{\left(r_k^{(i_j)}, p_k^{(i_j)}\right)\right\}\right| = 1$, and $|\cdot|$ denotes the cardinality of the set.

If the existing probabilities are the same between the components, i.e., $r_k^{i_j} = r_k^{i_m}$, and the distance between the Bernoulli components is within the threshold, then the two components are combined into a new one, the details are depending on $p_k^{i_j}$ and $p_k^{i_m}$, the specific algorithm is given in Algorithm 2.

Algorithm 2 gives the implements of merging algorithm to merge trajectories. Suppose that the MB filter eliminate the components whose existing probability below the threshold H_{merge} after the update step and the total number of Bernoulli components is within $T_{\max}$.

Algorithm 2 Track Merging algorithm pseudocode

Input: $\pi_k = \left\{\left(r_k^{(i)}, p_k^{(i)}\right)\right\}_{i=1}^{M_{k|k}}$
Set the truncation threshold as T_{trune} and truncate the particles in the Bernoulli component.
Resampling of the truncated Bernoulli components.
if $M_{k|k} > 1$ **then**
    Choose the two Bernoulli components $\left(r_k^{(l)}, p_k^{(l)}\right)$ and $\left(r_k^{(m)}, p_k^{(m)}\right)$, Calculate the position of the Bernoulli components, which are noted as A and B respectively.
else
    if $A - B < T_{th}$ and $r_k^{(l)} \neq r_k^{(m)}$ **then**
        retain Bernoulli component with higher probability of existence.
        Else if $A - B < T_{th}$ and $r_k^{(l)} = r_k^{(m)}$
        The two clusters of Bernoulli components have the same probability of existence, merge the two Bernoulli components, resample and select T_{trune} particles to construct the new Bernoulli component.
    else
        Retain $\left(r_k^{(m)}, p_k^{(m)}\right)$ and $\left(r_k^{(l)}, p_k^{(l)}\right)$, which are considered as two independent components.
    end if
    Only one updated component at time k is output.
end if
Output: $\pi_k = \left\{\left(r_k^{(i)}, p_k^{(i)}\right)\right\}_{i=1}^{M'_{k|k}}$

Note: Step 2 truncates the particles in each component and discard particles with low weights to avoid errors in the target estimation process. Step 3 is to resample the truncated particles and select the particles with high weights to represent the Bernoulli components. Step 7–13 is to remerge the probability densities of the hypothetical components with the same probability within the threshold to obtain the new components, and the components outside the threshold are retained.

4.3 SMC implementation of MB-TBD filtering with target amplitude fluctuations

In this section, the SMC implementation of the amplitude fluctuation target MB-TBD is given.

SMC Prediction: Given a MB posterior density $\pi_{k-1} = \left\{\left(r_{k-1}^{(i)}, p_{k-1}^{(i)}\right)\right\}_{i=1}^{M_{k-1}}$ at time $k-1$, each spatial probability density $p_{k-1}^{(i)}, i = 1, \ldots, M_{k-1}$ can be represented by a set of particles with weights $\left\{w_{k-1}^{(i,j)}, x_{k-1}^{(i,j)}\right\}_{j=1}^{L_{k-1}^{(i)}}$, i.e.,

$$p_{k-1}^{(i)}(\boldsymbol{x}) = \sum_{j=1}^{L_{k-1}^{(i)}} w_{k-1}^{(i,j)} \delta_{\boldsymbol{x}_{k-1}^{(i,j)}}(\boldsymbol{x}) \tag{43}$$

Then the predicted multi-Bernoulli density $\pi_{k|k-1} = \left\{\left(r_{P,k|k-1}^{(i)}, p_{P,k|k-1}^{(i)}\right)\right\}_{i=1}^{M_{k-1}} \cup \left\{\left(r_{\Gamma,k}^{(i)}, p_{\Gamma,k}^{(i)}\right)\right\}_{i=1}^{M_{\Gamma,k}}$ can be expressed as follows

$$r_{P,k|k-1}^{(i)} = r_{k-1}^{(i)} \sum_{j=1}^{L_{k-1}^{(i)}} w_{k-1}^{(i,j)} p_{S,k}\left(\boldsymbol{x}_{k-1}^{(i,j)}\right) \tag{44}$$

$$p_{P,k|k-1}^{(i)}(\boldsymbol{x}) = \sum_{j=1}^{L_{k-1}^{(i)}} \tilde{w}_{P,k|k-1}^{(i,j)} \delta_{\boldsymbol{x}_{P,k|k-1}^{(i,j)}}(\boldsymbol{x}) \tag{45}$$

$$\boldsymbol{x}_{P,k|k-1}^{(i,j)} \sim q_k^{(i)}\left(\cdot \mid \boldsymbol{x}_{k-1}^{(i,j)}, \boldsymbol{Z}_k\right), \quad j = 1, \ldots, L_{k-1}^{(i)} \tag{46}$$

$$w_{P,k|k-1}^{(i,j)} = \frac{w_{k-1}^{(i,j)} f_{k|k-1}\left(\boldsymbol{x}_{P,k|k-1}^{(i,j)} \mid \boldsymbol{x}_{k-1}^{(i,j)}\right) p_{S,k}\left(\boldsymbol{x}_{k-1}^{(i,j)}\right)}{q_k^{(i)}\left(\boldsymbol{x}_{P,k|k-1}^{(i,j)} \mid \boldsymbol{x}_{k-1}^{(i,j)}, \boldsymbol{Z}_k\right)} \tag{47}$$

$$\tilde{w}_{P,k|k-1}^{(i,j)} = w_{P,k|k-1}^{(i,j)} \Big/ \sum_{j=1}^{L_{k-1}^{(i)}} w_{P,k|k-1}^{(i,j)} \tag{48}$$

The birth Bernoulli component $\left\{\left(r_{\Gamma,k}^{(i)}, p_{\Gamma,k}^{(i)}\right)\right\}_{i=1}^{M_{\Gamma,k}}$ is given by the LABer-STC-TBD algorithm.

SMC Update: Given the predicted MB density $\pi_{k|k-1} = \left\{\left(r_{k|k-1}^{(i)}, p_{k|k-1}^{(i)}\right)\right\}_{i=1}^{M_{k|k-1}}$ at time k, each spatial probability density $p_{k|k-1}^{(i)}, i = 1, \ldots, M_{k|k-1}$ can be represented by a set of particles with weights $\left\{w_{k|k-1}^{(i,j)}, x_{k|k-1}^{(i,j)}\right\}_{j=1}^{L_{k|k-1}^{(i)}}$, i.e.,

$$p_{k|k-1}^{(i)}(\boldsymbol{x}) = \sum_{j=1}^{L_{k|k-1}^{(i)}} w_{k|k-1}^{(i,j)} \delta_{\boldsymbol{x}_{k|k-1}^{(i,j)}}(\boldsymbol{x}) \tag{49}$$

Then the updated multi-Bernoulli multi-target density $\pi_k = \left\{\left(r_k^{(i)}, p_k^{(i)}\right)\right\}_{i=1}^{M_{k|k-1}}$ can be expressed as

$$r_k^{(i)} = \frac{r_{k|k-1}^{(i)} \varrho_k^{(i)}}{1 - r_{k|k-1}^{(i)} + r_{k|k-1}^{(i)} \varrho_k^{(i)}} \tag{50}$$

$$p_k^{(i)} = \frac{1}{\varrho_k^{(i)}} \sum_{j=1}^{L_{k|k-1}^{(i)}} w_{k|k-1}^{(i,j)} L_z\left(\boldsymbol{Z}_k | \boldsymbol{x}_{k|k-1}^{(i,j)}\right) \delta_{\boldsymbol{x}_{k|k-1}^{(i,j)}}(\boldsymbol{x}) \tag{51}$$

where $\varrho_k^{(i)} = \sum_{j=1}^{L_{k|k-1}^{(i)}} w_{k|k-1}^{(i,j)} L_z\left(\boldsymbol{Z}_k | \boldsymbol{x}_{k|k-1}^{(i,j)}\right)$. Note that in this paper $L_z\left(\boldsymbol{Z}_k | \boldsymbol{x}_{k|k-1}^{(i,j)}\right)$ is CLR in section 3.1, and for SLR $L_z\left(|\boldsymbol{Z}_k|^2 | \boldsymbol{x}_{k|k-1}^{(i,j)}\right)$ in section 3.2. Select the likelihood ratio under different measurement type and fluctuation type as needed.

Resampling and Implementation Issue: Analogous to the standard multi-Bernoulli filter, each Bernoulli component resamples the particles follow the update step, in order to reduce the increasing number of trajectories, the components whose existence probability lower than the threshold H_{merge} are discarded. However, this cannot accurately estimate the number of Bernoulli components, especially when the birth Bernoulli component can also accurately estimate the true position of the target, it will produce cardinality bias.

5 Experiments

This paper addresses the detection and tracking of fluctuating targets such as stealth aircraft for range-bearing surveillance radar. The Swerling model is more effective for missiles and aircraft. In this section, the effectiveness of the method is verified by Monte Carlo simulation experiments.

5.1 Measurement model parameters and multi-objective error estimation

Assume that the noise covariance is $\Gamma = 2\sigma_n^2 I_{N_c}$, SNR $= 10\log_{10}\left(\frac{\mathrm{E}(\rho_k^2)}{2\sigma_n^2}\right)$, $r_{\min} = 100\,\text{km}$, $r_{\max} = 120\,\text{km}$, $\theta_{\min} = -75°$, $\theta_{\max} = 75°$, $N_r = 300$, $N_\theta = 100$, $\sigma^2 = 0.5$, $B = 150\,\text{KHz}$, $T_e = 6.67 \times 10^{-5}\,\text{s}$, $N_a = 55$, $\lambda = 3\,\text{cm}$, $c = 3 \times 10^8\,\text{m/s}$. In this paper, $\mathrm{E}\left[\rho_{k,i}^2\right] = \mathrm{E}\left[\rho_k^2\right]$

The Optimal Sub-pattern Assignment (OSPA) [30] is used to evaluate the performance of the algorithm, and the OSPA metric evaluates the estimation error of the

number of targets and the estimation error of the position of the targets for the multi-target filter. Consider now two sets $X = \{x_1, x_2, \ldots x_m\}$ and $Y = \{y_1, y_2, \ldots y_n\}$, where $m, n \in \mathbb{N}_0 = \{0, 1, 2, \ldots\}$. Let $d^{(c)}(x, y) = \min\left(c, \|x - y\|\right)$, and $\prod_n$ denote the set of permutations on $\{1, 2, \ldots, n\}$. Then, for $p \geq 1$, $c > 0$, if $m \leq n$, OSPA is defined as follows [37]

$$\bar{d}_p^{(c)}(X, Y) = \left[\frac{1}{n}\left(\min_{\pi \in \Pi_n} \sum_{i=1}^{m} \left(d^{(c)}(x_i, y_{\pi(i)})\right)^p + (n - m) \cdot c^p\right)\right]^{1/\mathrm{p}} \tag{52}$$

if $m > n$, $\bar{d}_p^{(c)}(X, Y) = \bar{d}_p^{(c)}(Y, X)$ and $\bar{d}_p^{(c)}(X, Y) = \bar{d}_p^{(c)}(Y, X) = 0$ if $m = n = 0$.

In the simulation experiments of this paper, set $p = 1, c = 1000$. The smaller the OSPA value, the more accurately the number of targets and the state estimation are indicated.

5.2 Scenario 1: experiments comparing LABer-STC-TBD and KpMB-TBD algorithms

Suppose that targets move in a straight line at a constant speed, there are three targets in the whole scenario, the duration is $K = 30\,s$, the targets are initialized at different positions, the target state includes plane position and velocity, the model is given by the following equation

$$\boldsymbol{x}_k = F\boldsymbol{x}_{k-1} + \boldsymbol{v}_{k-1} \tag{53}$$

where $F = \begin{bmatrix} F_s & 0 \\ 0 & F_s \end{bmatrix}$, $F_s = \begin{bmatrix} 1 & T \\ 0 & 1 \end{bmatrix}$, $\boldsymbol{v}_k \sim \mathcal{N}(\cdot; 0, \sigma_v^2 Q)$, $\sigma_v = 5\,\mathrm{m/s}^2$, $Q = \begin{bmatrix} \frac{T^2}{2} & T & 0 & 0 \\ 0 & 0 & \frac{T^2}{2} & T \end{bmatrix}^{\mathrm{T}} \sigma_v^2$.

To verify the broadness and effectiveness of the LABer-STC-TBD algorithm as well as the track merging algorithm in the case of target amplitude fluctuations, the LABer-STC-TBD algorithm and the KpMB-TBD algorithm are used to detect and estimate multiple targets based on different amplitude fluctuations. The multi-Bernoulli density of the birth process is

$$\pi_\Gamma = \left\{\left(r_\Gamma, p_\Gamma^{(i)}\right)\right\}_{i=1}^{3} \tag{54}$$

where $p_\Gamma^{(i)}(x) = \mathcal{N}\left(x; m_\gamma^{(i)}, P_\gamma\right)$,
$\boldsymbol{m}_\gamma^{(1)} = [94000, 0, 9000, 0]^{\mathrm{T}}$,
$\boldsymbol{m}_\gamma^{(2)} = [-177000, 0, -51000, 0]^{\mathrm{T}}$,
$\boldsymbol{m}_\gamma^{(3)} = [148300, 0, -23500, 0]^{\mathrm{T}}$,
$r_\Gamma = 0.1$, $P_\gamma = \mathrm{diag}\left([1000, 500, 1000, 500]^{\mathrm{T}}\right)^2$.

The real trajectory on the two-dimensional plane is shown in Fig. 5, and the initial position of the target is shown in Table 1.

In SNR=9dB, the number of particles for each new birth Bernoulli component is 1000, and the algorithm simulations are compared under different amplitude fluctuations using 100 Monte Carlo experimental simulations. The LABer-STC-TBD algorithm is compared with the KpBer-TBD algorithm implementation under different amplitude fluctuations considering four filters as follows.

1 The first filter, labeled as "LA-STC-Com", considers the LABer-STC-TBD algorithm under multi-Bernoulli filter CLR.
2 The second filter, labeled as "LA-STC-Squ", considers the LABer-STC-TBD algorithm under the multi-Bernoulli filter SLR.
3 The third filter, labeled as "Kp-Com", considers the KpBer-TBD algorithm with multi-Bernoulli filter CLR.
4 The fourth filter, labeled as "Kp-Squ", considers the KpBer-TBD algorithm with multi-Bernoulli filter SLR.

The results are shown in Figs. 6, 7 and 8. To verify the reasonableness of the results, 100 Monte Carlo experiments were conducted and averaged, and Figs. 6, 7 and 8 represent the LABer-STC-TBD algorithm and KpBer-TBD algorithm for two likelihood ratio calculations under three amplitude fluctuation types Swerling 0, 1, 3, based on the Monte Carlo average OSPA distance estimation error and the average number of targets. The results confirm that the LABer-STC-TBD algorithm can accurately estimate the positions and number of targets, although the estimation error of the KpBer-TBD algorithm is smaller than that of the LABer-STC-TBD algorithm at the initial moment, but the error increases rapidly and eventually show a divergence. The reason is that the KpBer-TBD algorithm is given the correct initialization and the prediction of the state transfer equation happens to be close to the true state for the initial few moments, after which the target state prediction decreases as noise as well as uncertainties such as clutter interfere, eventually leading to worse and worse tracking and higher and higher errors. The same is true for the estimation of the number of targets. In the process of target amplitude fluctuation, the target echoes will be completely annihilated in the noise part of the time, and the LABer-STC-TBD algorithm will use the previous moment's measurement information to search for the true target location as much as possible, making the estimated number accurate and the filter can keep iterating even if the noise

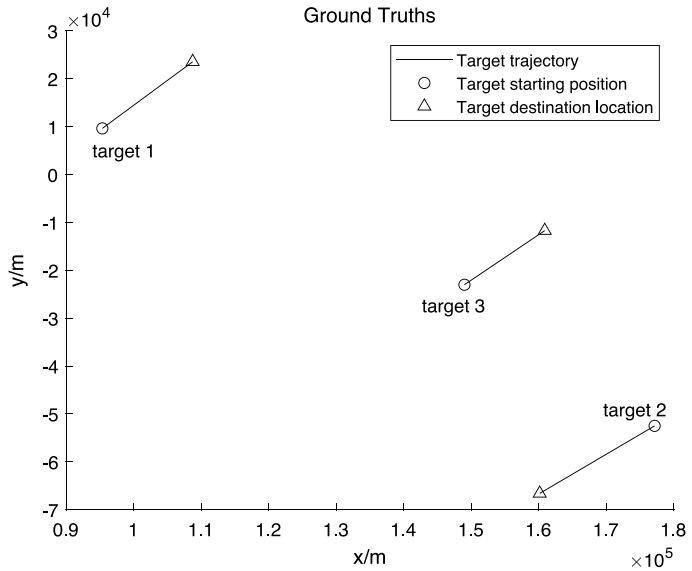

Fig. 5 True trajectories of 3 targets on the 2D plane

Table 1 The initial position of the targets

Target initial state	Appearance time (s)	Disappearance time (s)
$\boldsymbol{x}_1 = [94815; 535; 9088; 557]$	1	26
$\boldsymbol{x}_2 = [177827; -681; -51916; -564]$	5	30
$\boldsymbol{x}_3 = [148390; 595; -23569; 565]$	10	30

drowns out all the target information at a certain moment. If the KpBer-TBD algorithm does not estimate the target at a certain moment effectively, and the target is moving faster, the target will not be estimated at the next moment, resulting in the failure of the filter. And Figs. 6, 7 and 8 also show that the filter with the CLR outperforms the filter with the SLR.

Comparing these four filter algorithms from Figs.6, 7 and 8, the LABer-STC-TBD algorithm under the CLR has the best effect, proving that the phase information can improve the detection tracking performance of the MeMBer-TBD algorithm, and the selection of the measurement threshold of the birth algorithm reduces the computational complexity, and the selected measurements generated by the real targets are based on the target amplitude, to the largest degree. Using the likelihood ratio to select Bernoulli components to eliminate the wrong estimation at the previous moment, the STC idea is introduced to avoid the influence of strong and weak echoes of the target at the same moment and to maximize the exploitation of the target echo information. From Figs. 7b and 8b, it can be seen that the LABer-STC-TBD with SLR is not accurate for target number estimation in the target with amplitude fluctuation type Swerling 1,3, due to the fact that the square measure ignore the phase information of the target, and comparing with Fig. 6b, it can be seen that the loss of phase information is extremely obvious for fluctuating targets.

5.3 Scenario 2: experiments comparing the likelihood ratios of CLR and SLR in MB-TBD

Scenario 5.2 demonstrates the advantages of the LABer-STC-TBD algorithm in the MB-TBD with amplitude fluctuations, and the tracking effect of the CLR is better than the SLR in the target tracking process under the same conditions. To further compare the advantages and disadvantages of the CLR and SLR as well as the reasonableness and superiority of the LABer-STC-TBD algorithm in the MB-TBD, targets are assumed to make a turn at a constant speed. There are five targets in the whole scenario, the time duration is $K = 100\,s$, the targets are initialized at different positions, and the target state variables is $\boldsymbol{x}_k = \left[\tilde{\boldsymbol{x}}_k^T, \omega_k\right]^{\mathrm{T}}$ include the plane position as well as the velocity is $\tilde{\boldsymbol{x}}_k^{\mathrm{T}} = \left[p_{x,k}, \dot{p}_{x,k}, p_{y,k}, \dot{p}_{y,k}\right]^{\mathrm{T}}$ and the turn rate is ω_k. The state transfer model is

$$\tilde{\boldsymbol{x}}_k = F\left(\boldsymbol{\omega}_{k-1}\right)\tilde{\boldsymbol{x}}_{k-1} + G\boldsymbol{\omega}_{k-1} \tag{55}$$

$$\boldsymbol{\omega}_k = \boldsymbol{\omega}_{k-1} + \Delta\boldsymbol{u}_{k-1} \tag{56}$$

where

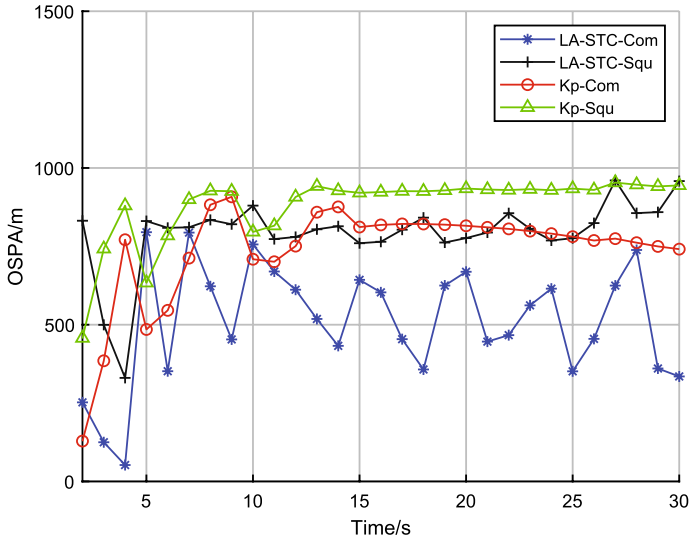

(a) OSPA distance error

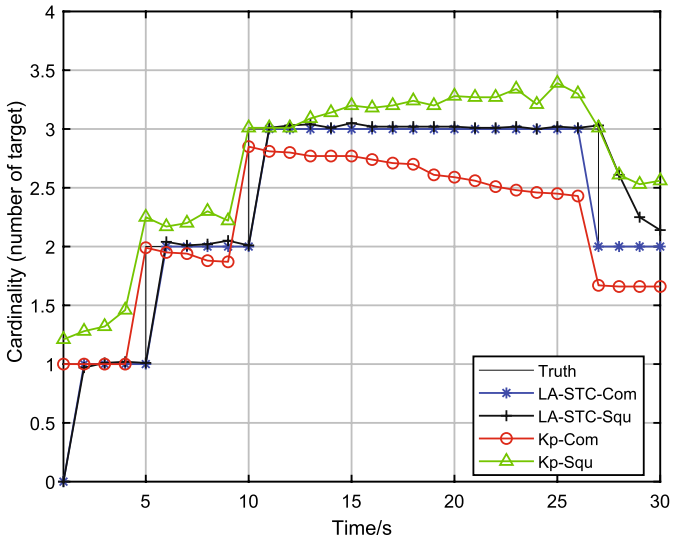

(b) Estimated target number

Fig. 6 Comparison of LABer-STC-TBD algorithm and KpBer-TBD algorithm under Swerling 0

$$F(\omega)=\begin{bmatrix}1 & \frac{\sin\omega\Delta}{\omega} & 0 & -\frac{1-\cos\omega\Delta}{\omega}\\ 0 & \cos\omega\Delta & 0 & -\sin\omega\Delta\\ 0 & \frac{1-\cos\omega\Delta}{\omega} & 1 & \frac{\sin\omega\Delta}{\omega}\\ 0 & \sin\omega\Delta & 0 & \cos\omega\Delta\end{bmatrix},$$

$G=\begin{bmatrix}\frac{\Delta^2}{2} & 0\\ T & 0\\ 0 & \frac{\Delta^2}{2}\\ 0 & T\end{bmatrix}$, $\boldsymbol{\omega}_{k-1}\sim\mathcal{N}(\cdot;0,\sigma_\omega^2 I)$, $\boldsymbol{u}_{k-1}\sim\mathcal{N}(\cdot;0,\sigma_u^2 I)$, $\Delta=1s$, $\sigma_\omega=15\,\mathrm{m/s^2}$, and $\sigma_u=\pi/180\,\mathrm{m/s^2}$

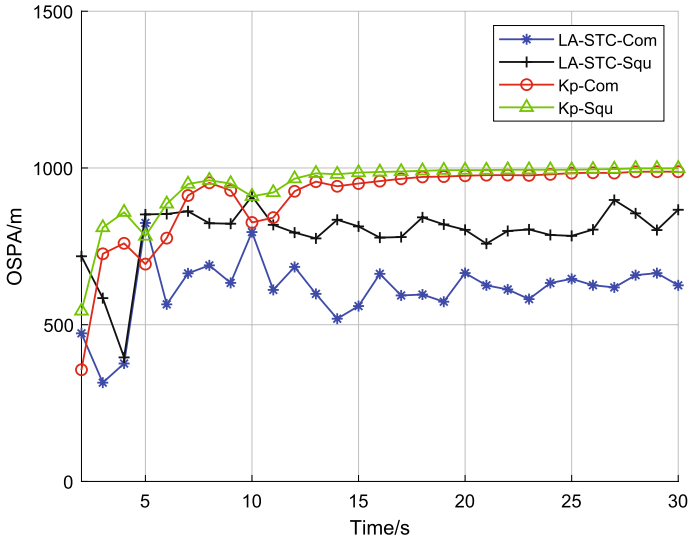

(a) OSPA distance error

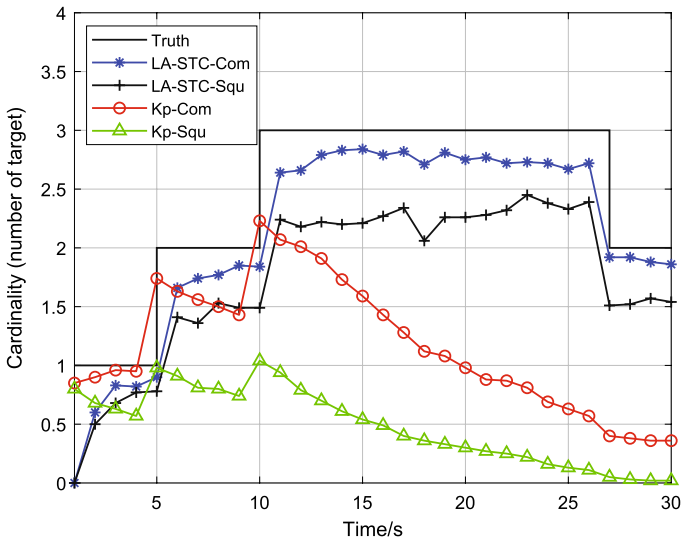

(b) Estimated target number

Fig. 7 Comparison of LABer-STC-TBD algorithm and KpBer-TBD algorithm under Swerling 1

Figure 9 shows the real trajectory on a two-dimensional plane. Different targets have different turn rates, and the initial position of the target is shown in Table 2, where wturn $= \frac{2\pi}{180}$.

The targets are tracked in two scenarios with SNR $= 7$ dB and SNR $= 5$ dB, and the number of particles of each birth Bernoulli component is 1000, using 100 Monte Carlo experimental simulations to compare algorithmic simulations considering the LABer-STC-TBD algorithm under different amplitude fluctuations. The following two filters are considered.

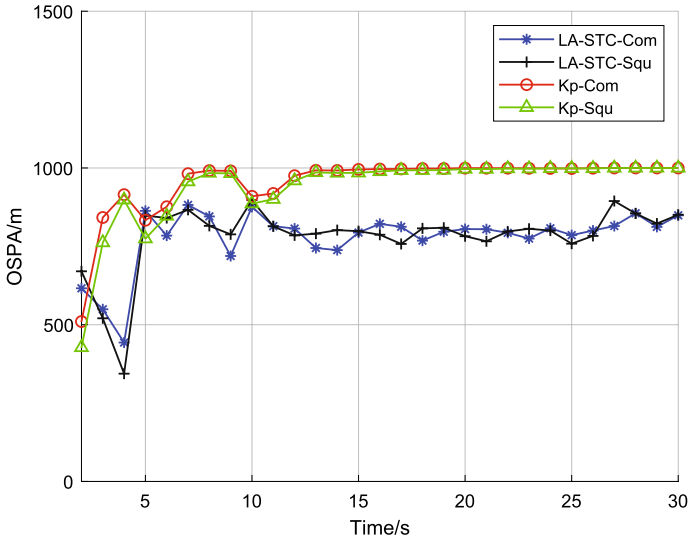

(a) OSPA distance error

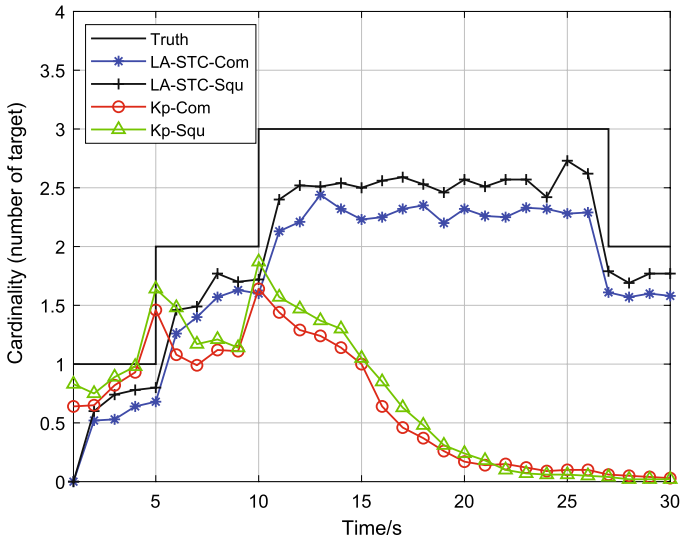

(b) Estimated target number

Fig. 8 Comparison of LABer-STC-TBD algorithm and KpBer-TBD algorithm under Swerling 3

1 The first filter labeled as "Comp mod", considers the LABer-STC-TBD filter under CLR.
2 The second filter labeled as "Sq mod", considers the LABer-STC-TBD filter under SLR.

The results are shown in Figs. 10, 11 and 12.

The detection performance of different MB-TBD strategies for Swerling type 0, 1, 3 targets is shown from Figs. 10, 11 and 12, respectively. The advantage of the CLR algorithm at low SNR ratio is verified, and for all detection results, the LABer-STC-TBD

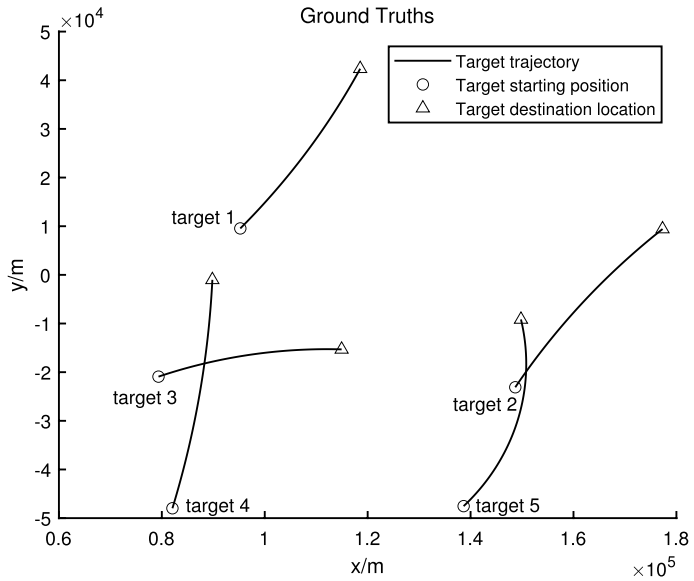

Fig. 9 True trajectories of 5 targets on the 2D plane

Table 2 The initial position of the targets

Target initial state	Appearance time (s)	Disappearance time (s)	Turn rate (rad/s)
$\tilde{\boldsymbol{x}}_1 = [94815; 435; 9088; 457]$	1	65	wturn/8
$\tilde{\boldsymbol{x}}_2 = [148390; 295; -23569; 465]$	1	80	− wturn/9
$\tilde{\boldsymbol{x}}_3 = [78949; 401; -21061; 145]$	5	90	− wturn/8
$\tilde{\boldsymbol{x}}_4 = [81837; 223; -48736; 763]$	40	100	wturn/9
$\tilde{\boldsymbol{x}}_5 = [138136; 519; -48036; 498]$	42	100	wturn/2

using the CLR outperforms the LABer-STC-TBD using the SLR. The introduction of the phase information improves the system performance, which makes it possible to detect and track the target more accurately at low SNR. Moreover, under the same fluctuation, the CLR only needs to perform the calculation of Bessel function once, while the SLR needs to perform multiple Bessel functions, which effectively reduces the computational complexity.

Figure 10 shows the performance of LABer-STC-TBD algorithm with no fluctuations in the target, and both SLR and CLR can estimate the target state and the number of targets more accurately. Figures 11 and 12 show performance of the LABer-STC-TBD algorithm with fluctuation type Swerling 1, 3, which reflects the advantage of the CLR over the SLR. However, in the case of low SNR, the estimated number of targets is often lower than the true number of targets, the reason is that the fluctuation of the target amplitude lead to the targets annihilated in the noise.

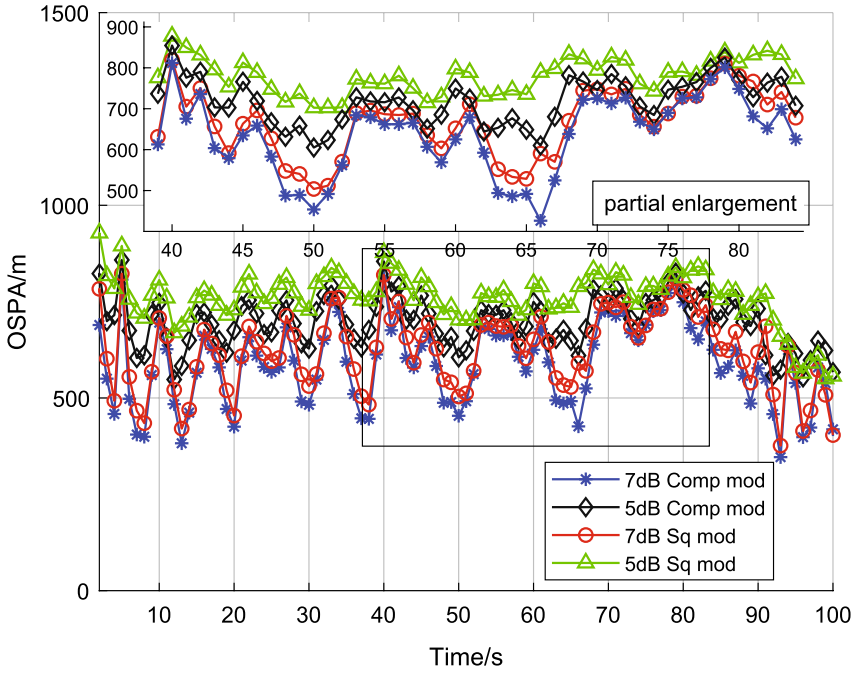

(a) OSPA distance error

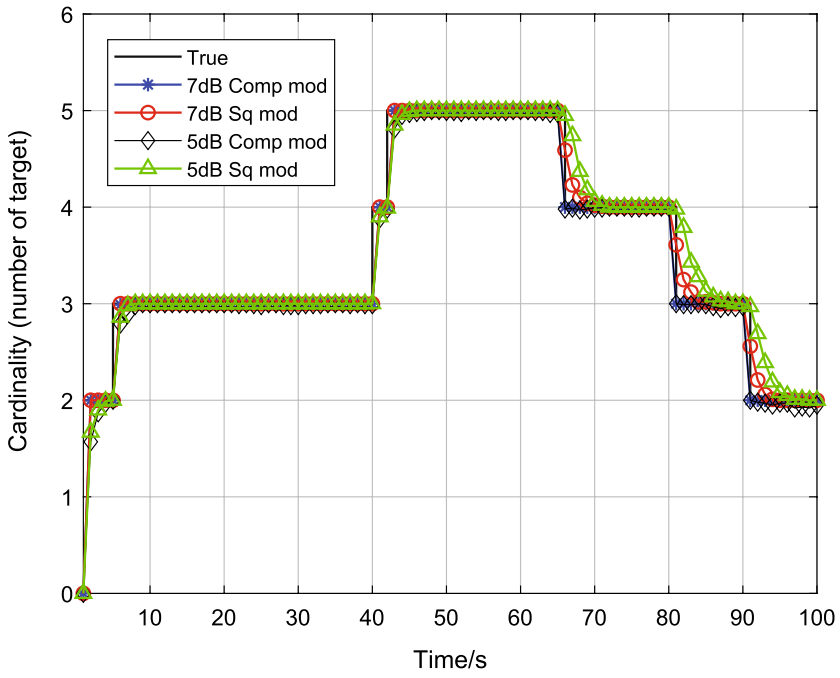

(b) Estimated target number

Fig. 10 Two likelihood ratio algorithms with different SNR ratios under Swerling 0

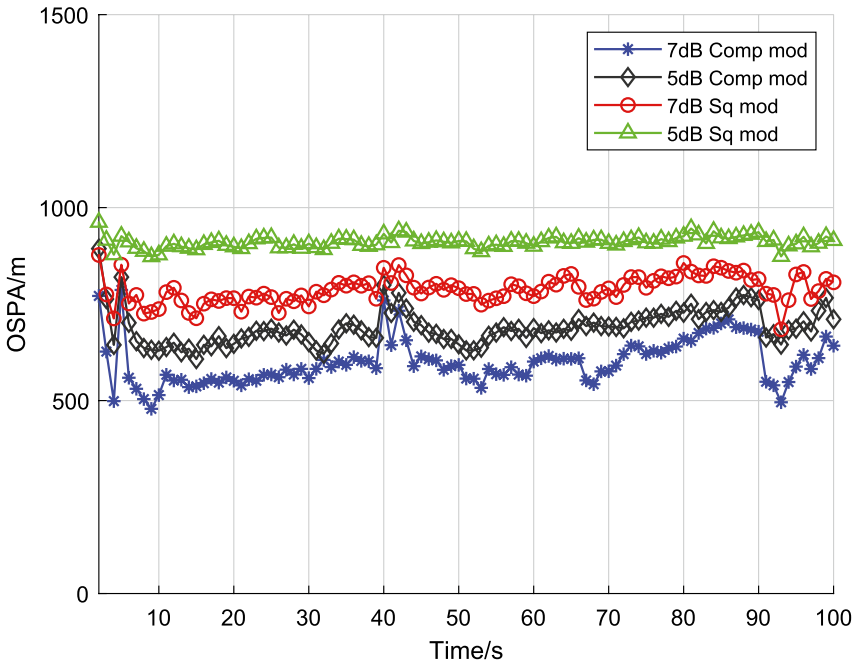

(a) OSPA distance error

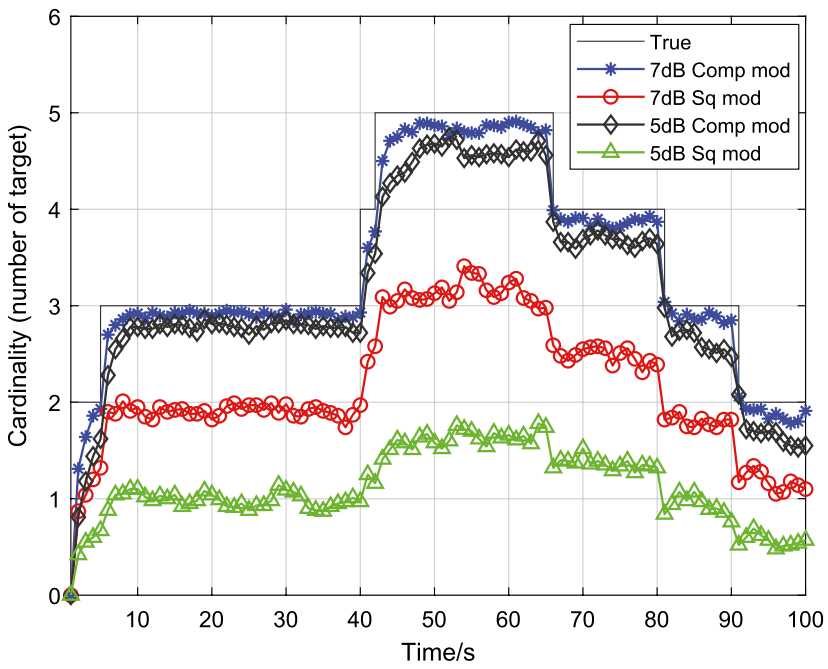

(b) Estimated target number

Fig. 11 Two likelihood ratio algorithms with different SNR ratios under Swerling 1

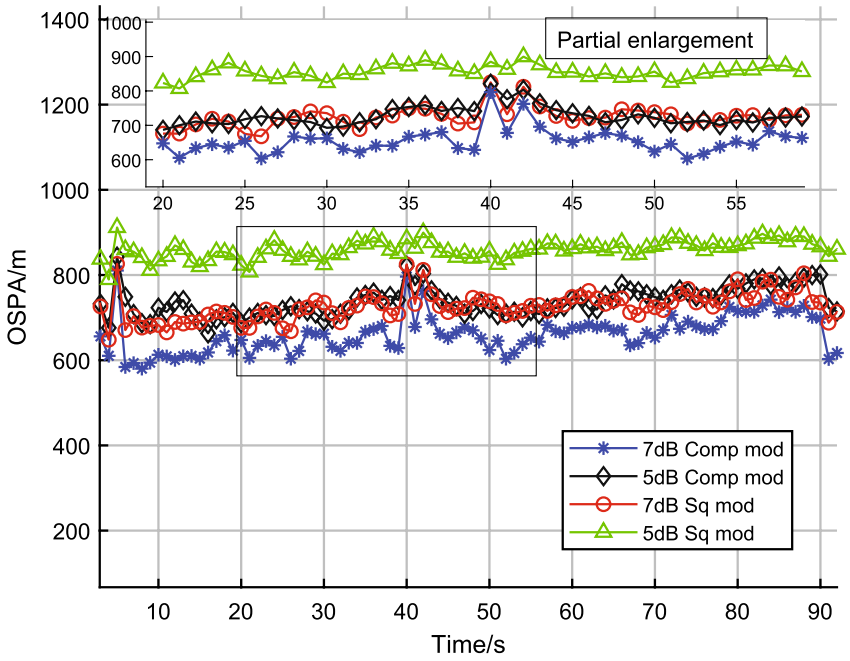

(a) OSPA distance error

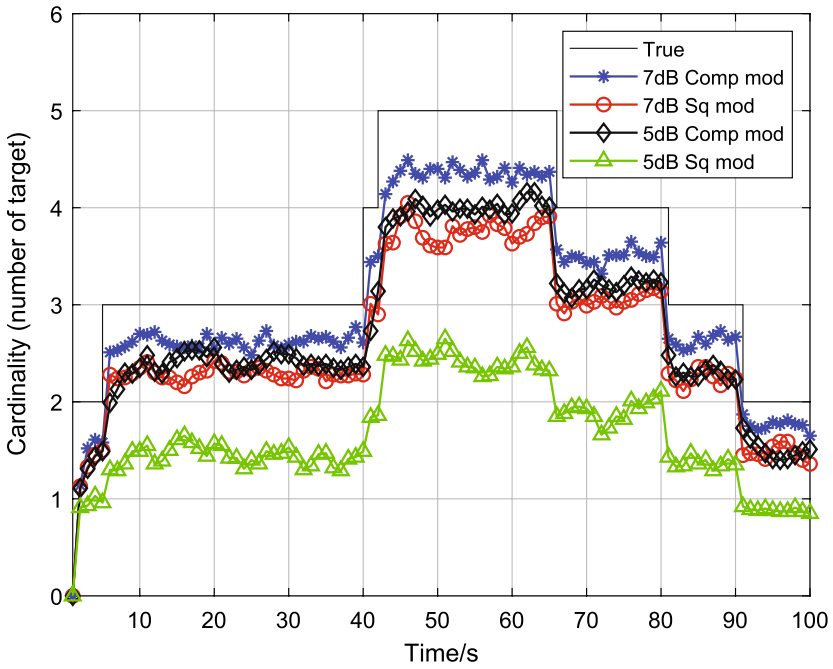

(b) Estimated target number

Fig. 12 Two likelihood ratio algorithms with different SNR ratios under Swerling 3

6 Results and discussion

It can be seen from the above experiments that the CLR method can improve the detection and tracking performance of weak multi-targets. Under the low SNR, the robustness of CLR is better than that of SLR, as shown in Figs. 10, 11 and 12. At the same time, when the target fluctuates, the LABer-STC-TBD algorithm solves the problem of detection failure during the fluctuation process and the situation that the birth prior information of the target is unknown, as shown in Figs. 6, 7 and 8.

It should be noted that, with the development of radar targets, stealth targets, high-speed flying targets, etc., the classical Swrling model can no longer accurately represent the statistical performance of various targets. At the same time, the RCS of complex targets is sensitive to changes in frequency and attitude angle, and the RCS of complex targets does not maintain a single statistical distribution in any frequency band and under any attitude. Our research is mainly based on the characteristics of radar measurement to improve the detection performance of the target. The next work will deal with the limitations encountered above and solve practical problems in a reasonable range.

7 Conclusion

In this paper, the multi-Bernoulli filter based on track-before-detect for target amplitude fluctuation problem is investigated under range-bearing surveillance radar. Three different Swerling target amplitude fluctuation models are considered. In order to improve the detection performance of MB-TBD, not only the amplitude information of target is considered, but also the phase information is processed. The following conclusions are obtained through simulation: (a) For the same fluctuating target model, MB-TBD filter using CLR outperforms the one using SLR, and the former has better detection and tracking performance for multi-targets at low SNR scenarios. (b) The proposed LABer-STC-TBD algorithm mainly solves two types of difficulties in the target fluctuation problem, one is to solve the problem of unknown prior information about the target birth, and the other is the problem of possible filter ineffectiveness when the targets fluctuation. (c) The proposed merge algorithm solves the problem of linear growth of the components after the MB-TBD filter update. Although the Swerling 1, 3 model is no longer very suitable for modern aircraft, changing the degrees of freedom can fit other fluctuation target models, and this paper has some reference significance for the detection and tracking of targets such as stealth aircraft. In practical application, the most suitable fluctuation model should be chosen according to the fluctuation characteristics of the target.

Abbreviations

MB-TBD	Track-before-detect algorithm based on multi-Bernoulli
CLR	Complex likelihood ratios
SLR	Squared modulus measurements likelihood ratios
MTT	Multi-target tracking
RCS	Radar cross section
TBD	Track-before-detect
DP	Dynamic programming
PF	Particle filtering
RFS	Random finite set
PHD	Probability hypothesis density
CPHD	Cardinalized PHD
SNR	Signal noise ratio

MLRF	Measurement likelihood ratio function
STC	Successive-target-cancellation
LABer-STC-TBD	Joint measurement likelihood ratio driven and successive-target cancellation (STC)-based adaptive birth distribution for MB-TBD
KpMB-TBD	The MB-TBD with a priori knowledge
OSPA	The Optimal Sub-pattern Assignment
LA-STC-Com	The LABer-STC-TBD algorithm under multi-Bernoulli filter CLR
LA-STC-Squ	The LABer-STC-TBD algorithm under the multi-Bernoulli filter SLR
Kp-Com	The KpBer-TBD algorithm with multi-Bernoulli filter CLR
Kp-Squ	The KpBer-TBD algorithm with multi-Bernoulli filter SLR
Comp mod	The LABer-STC-TBD filter under CLR
Sq mod	The LABer-STC-TBD filter under SLR

Author contributions
All authors have contributed toward this work as well as in compilation of this manuscript. All authors read and approved the final manuscript.

Funding
This work was supported in part by the National Natural Science Foundation of China (61861008, 62061010, 62161007), in part by the Guangxi Science and Technology Department project (AA19182007, AA19254029, AA20302022, AB21196041), in part by Guangxi Natural Science Foundation 2019GXNSFBA245072, in part by Guangxi Key Laboratory of Cryptography and Information Security (NoGCIS202132).

Availability of dat anad materials
The datasets used and analyzed during the current study are available from the corresponding author on reasonable request.

Declarations

Ethics approval and consent to participate
Not applicable.

Consent for publication
We agree to the publication of the paper.

Competing interests
The authors declare that they have no competing interests.

Received: 19 March 2022 Accepted: 21 June 2022
Published online: 09 July 2022

References

1. Y. Bar-Shalom, F. Daum, J. Huang, The probabilistic data association filter. IEEE Control Syst. **29**(6), 82–100 (2010). https://doi.org/10.1109/MCS.2009.934469
2. M.S. Arulampalam, S. Maskell, N. Gordon, T. Clapp, A tutorial on particle filters for on-line nonlinear/non-Gaussian Bayesian tracking. IEEE Trans. Signal Process. **50**(2), 174–188 (2002). https://doi.org/10.1049/ic:20010246
3. Y. Bar-Shalom, W.D. Blair, *Multitarget–Multisensor Tracking: Applications and Advances*, vol. 3 (Artech House, Norwood, 2007)
4. H.C. Jiang, W. Yi, G.L. Cui, L.J. Kong, X.B. Yang, Track-before-detect for fluctuating targets using phase information, in *2015 IEEE Radar Conference* (2015), pp. 0344–0349. https://doi.org/10.1109/RADAR.2015.7131022
5. E. Grossi, M. Lops, L. Venturino, A track-before-detect algorithm with thresholded observations and closely-spaced targets. IEEE Signal Process. Lett. **20**(12), 1171–1174 (2013). https://doi.org/10.1109/LSP.2013.2283586
6. J.Y.H. Wang, X. Wan, Greedy algorithm-based track-before-detect in radar systems. IEEE Sens. J. **18**(17), 7158–7165 (2018). https://doi.org/10.1109/JSEN.2018.2853188
7. H.C. Jiang, W. Yi, L. Kong, X. Yang, Knowledge-based track-before-detect strategies for fluctuating targets in k-distributed clutter. IEEE Sens. J. **16**(19), 7124–7132 (2016). https://doi.org/10.1109/JSEN.2016.2597320
8. Y. Boers, J.N. Driessen, Multitarget particle filter track before detect application. IEE Proc. Radar Sonar Navig. **151**(6), 351–357 (2004). https://doi.org/10.1049/ip-rsn:20040841
9. D.J. Salmond, H. Birch, A particle filter for track-before-detect. in *Proceedings of the 2001 American Control Conference (5)* (2001), pp. 3755–3760. https://doi.org/10.1109/ACC.2001.946220
10. F. Cai, H.Q. Fan, Q. Fu, Dual-channel particle filter based track-before-detect for monopulse radar. Math. Probl. Eng. (2014). https://doi.org/10.1155/2014/750279
11. R.P.S. Mahler, *Statistical Multisource–Multitarget Information Fusion* (Artech House, Inc., Norwood, 2007)
12. B.T. Vo, A.C.B.N. Vo, The cardinality balanced multitarget multi-Bernoulli filter and its implementations. IEEE Trans. Signal Process. **57**(2), 409–423 (2009)
13. B. Vo, N.P.D.S.B. Vo, Joint detection and estimation of multiple objects from image observations. IEEE Trans. Signal Process. **58**(10), 5129–5141 (2010). https://doi.org/10.1109/TSP.2010.2050482

14. R. Mahler, Multitarget Bayes filtering via first-order multitarget moments. IEEE Trans. Aerosp. Electron. Syst. **39**(4), 1152–1178 (2004). https://doi.org/10.1109/TAES.2003.1261119
15. S.S.B. Vo, Sequential Monte Carlo methods for multitarget filtering with random finite sets. IEEE Trans. Aerosp. Electron. Syst. **41**(4), 1224–1245 (2005). https://doi.org/10.1109/TAES.2005.1561884
16. W.M.B. Vo, The gaussian mixture probability hypothesis density filter. IEEE Trans. Signal Process. **54**(11), 4091–4104 (2006). https://doi.org/10.1109/TSP.2006.881190
17. W.H. Wu, Z.L.H.J.J.X.M.Z.H.M. Sun, C. Chen, Multi-GMTI fusion for doppler blind zone suppression using PHD fusion. Signal Process. **183**, 108024 (2021). https://doi.org/10.1016/j.sigpro.2021.108024
18. W.H. Wu, W.J. Liu, J. Jiang, L. Gao, Q. Wei, C.Y. Liu, GM-PHD filter-based multi-target tracking in the presence of doppler blind zone. Digit. Signal Process. **52**, 1–12 (2026). https://doi.org/10.1016/j.dsp.2016.01.014
19. B. Vo, A.C.B. Vo, Analytic implementations of the cardinalized probability hypothesis density filter. IEEE Trans. Signal Process. **55**(7), 35533567 (2007). https://doi.org/10.1109/TSP.2007.894241
20. B. Vo, A.C.B. Vo, Bayesian filtering with random finite set observations. IEEE Trans. Signal Process. **56**(4), 1313–1326 (2018). https://doi.org/10.1109/TSP.2007.908968
21. X.L. Shen, Z.Y. Song, H. Fan, Q. Fu, Particle filter implementation of CPHD filter for unknown clutter, in *6th International Conference on Electrical Engineering and Informatics (ICEEI)*
22. W.H. Wu, H.M. Sun, Y. Cai, J.J. Xiong, MM-GLMB filter-based sensor control for tracking multiple maneuvering targets hidden in the doppler blind zone. IEEE Trans. Signal Process. **68**, 4555–4567 (2020). https://doi.org/10.1109/TSP.2020.3009497
23. W.H. Wu, H.M. Sun, Y.C. Cai, Tracking multiple maneuvering targets hidden in the DBZ based on the MM-GLMB filter. IEEE Trans. Signal Process. **68**, 2912–2924 (2020). https://doi.org/10.1109/TSP.2020.2988635
24. W.H Wu, H.M. Sun, W. Huang, M. Zheng, X. Feng, Multi-GMTI decentralized tracking via consensus LMB density fusion, in *2021 International Conference on Control, Automation and Information Sciences (ICCAIS)* (2021)
25. L. Chai, L.J. Kong, S.Q. Li, W. Yi, The multiple model multi-Bernoulli filter based track-before-detect using a likelihood based adaptive birth distribution. Signal Process. **171**, 107501 (2020). https://doi.org/10.1016/j.sigpro.2020.107501
26. F. Papi, B.T. Vo, M. Bocquel, B.N. Vo, Multi-target track-before-detect using labeled random finite set, in *2013 International Conference on Control, Automation and Information Sciences (ICCAIS)*, pp. 116–121
27. S.J. Davey, M.G. Rutten, B. Cheung, A comparison of detection performance for several track-before-detect algorithms, in *2008 11th International Conference on Information Fusion*, pp. 116–121
28. M.G. Rutten, N.J. Gordon, S. Maskell, Recursive track-before-detect with target amplitude fluctuations. IEE Proc. Radar Sonar Navig. **12**, 116–121 (2002). https://doi.org/10.1049/ip-rsn:20045041
29. S.J. Davey, M.G. Rutten, B. Cheung, Using phase to improve track-before-detect. IEEE Trans. Aerosp. Electron. Syst. **48**(1), 832–849 (2012). https://doi.org/10.1109/TAES.2012.6129673
30. A. Lepoutre, O. Rabaste, F.L. Gland, Multitarget likelihood computation for track-before-detect applications with amplitude fluctuations of type swerling 0, 1, and 3. IEEE Trans. Aerosp. Electron. Syst. **52**(3), 1089–1107 (2008). https://doi.org/10.1109/TAES.2016.140909
31. H.C. Jiang, W. Yi, T. Kirubarajan, L. Kong, X. Yang, Multiframe radar detection of fluctuating targets using phase information. IEEE Trans. Aerosp. Electron. Syst. **53**(2), 736–749 (2017). https://doi.org/10.1109/TAES.2017.2664639
32. M. Mcdonald, B. Balaji, Track-before-detect using swerling 0, 1, and 3 target models for small maneuvering maritime targets. EURASIP J. Adv. Signal Process. **2008**(1), 1–9 (2017). https://doi.org/10.1155/2008/326259
33. S. Reuter, D. Meissner, B. Wilking, K. Dietmayer, Cardinality balanced multi-target multi-Bernoulli filtering using adaptive birth distributions, in *Proceedings of the 16th International Conference on Information Fusion* (2013), pp. 1608–1615
34. N. Levanon, E. Mozeson, *Radar Signals* (Wiley, New York, 2004)
35. S. Buzzi, M. Lops, L. Venturino, M. Ferri, Track-before-detect procedures in a multi-target environment. IEEE Trans. Aerosp. Electron. Syst. **44**(3), 1135–1150 (2008). https://doi.org/10.1109/TAES.2008.4655369
36. A. Lepoutre, O. Rabaste, A particle filter for target arrival detection and tracking in track before-detect, in *2012 Workshop on Sensor Data Fusion: Trends, Solutions, Applications* (2012), pp. 13–18
37. B. Ristic, B.N. Vo, Sensor control for multi-object state-space estimation using random finite sets. Automatica **46**(11), 1812–1818 (2010). https://doi.org/10.1016/j.automatica.2010.06.045

Publisher's Note